Pre-print version

R. Donida Labati, and F. Scotti, "Noisy iris segmentation with boundary regularization and reflections removal", in *Image and Vision Computing, Iris Images Segmentation Special Issue*, Elsevier, pp. 270-277, February, 2010.

DOI: 10.1016/j.imavis.2009.05.004

Noisy Iris Segmentation with Boundary Regularization and Reflections Removal

Ruggero Donida Labati and Fabio Scotti

Università degli Studi di Milano

Department of Information Technologies, via Bramante 65, 26013 Crema (CR), Italy

Abstract *– The paper presents an innovative algorithm for the segmentation of the iris in noisy images, with boundaries regularization and the removal of the possible existing reflections. In particular, the method aims to extract the iris pattern from the eye image acquired at the visible wavelength, in an uncontrolled environment where reflections and occlusions can also be present, on-the-move and at variable distance. The method achieves the iris segmentation by the following three main steps. The first step locates the centers of the pupil and the iris in the input image. Then two image strips containing the iris boundaries are extracted and linearizated. The last step locates the iris boundary points in the strips and it performs a regularization operation by achieving the exclusion of the outliers and the interpolation of missing points. The obtained curves are then converted into the original image space in order to produce a first segmentation output. Occlusions such as reflections and eyelashes are then identified and removed from the final area of the segmentation. Results indicate that the presented approach is effective and suitable to deal with the iris acquisition in noisy environments. The proposed algorithm ranked seventh in the international Noisy Iris Challenge Evaluation (NICE.I).*

Keywords *– Iris segmentation, Boundary Regularization, Outliers removal, Reflections identification.*

1 INTRODUCTION

The diffusion of biometric systems is rapidly growing all over the word in a broad variety of fields ranging from the governance to the commercial applications. This huge variety of applicative contests [1] pushes the research toward new challenges such as the capability to guarantee accurate and reliable measures also in difficult and noisy environments [2]. In the case of iris recognition systems, the cooperation of the user, the acquisition setup and the environment are critical factors for a correct behavior of the recognition algorithms. One of the most critical steps in the iris-based recognition system is the localization of the iris pattern in the input image due to the great variability that can be present. An incomplete list of these factors encompasses the variability of the iris position in the eye, the eye position in the image, the presence of occlusions such as glasses, hairs, eyelashes, out-of-focus problems, blurring effects and superimposed reflections, and the great variability of iris sizes and color skins.

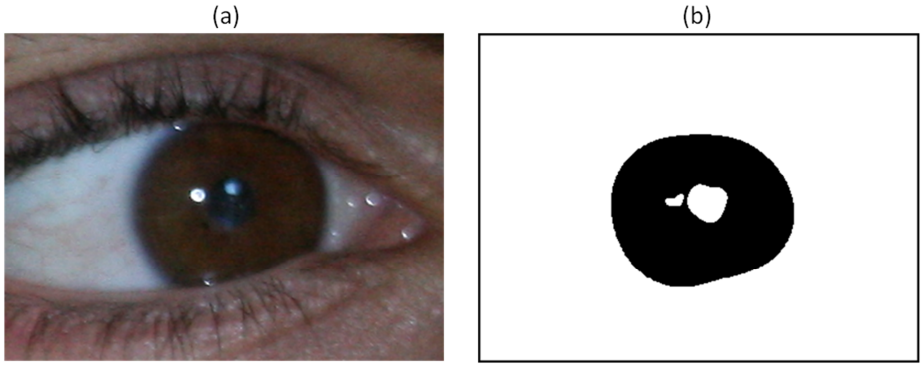

Fig.1: Processing the segmentation of the iris pattern: an example of input image (a), and the related segmented iris pattern (b).

The behavior of most traditional algorithms is often designed for controlled/low-noise environments and it is typically not satisfactory in noisy images, where specific methods are needed to successfully cope with this peculiar applicative contest. The work we propose deals with the segmentation of the iris patterns in this type of noisy images, with particular reference to the dataset NICE.I [3], a public database containing a broad collection of images taken in a great variety of acquisition conditions. Fig. 1 plots an example of an input image (Fig. 1a) and the output of the algorithm which is the segmented iris pattern (Fig. 1b) associated to the input image.

The paper is structured as follows. Section 2 presents the proposed method and its main steps: (i) the processing of the starting data (the centers and radii of the outer and inner boundaries of the iris), (ii) the extraction of two strips containing the internal and external boundaries of the iris, (iii) the processing of the extracted strips in order to obtain the candidate iris boundary points, (iv) the regularization of the iris boundaries, (v) the elimination of reflections and eyelashes superimposed to the iris pattern and (vi) the final reconstruction of the segmented area where the iris pattern is present. Section 3 presents the experimental results of the application of the presented method on the NICE.I dataset. It also discusses the results within the international competition NICE.I, by commenting the behavior of the proposed method in the best and worst segmented images in the dataset. In the last section, the paper resumes the proposed approach and it describes some further improvements and future works.

2 THE PROPOSED APPROACH

The algorithm we propose processes from an input image $I(x,y)$ a binary output image $O(x,y)$ where the pixels are set to zero if they belong to the iris pattern, otherwise they are set to one. The method can be partitioned in four main steps (Fig. 2). In the first step, the method estimates the position of the centers of the outer and inner boundary of the iris, and the two related radii. Then, two image strips containing the inner and outer iris boundary are extracted and linearizated. The third step consists in the estimation of the iris boundary points into the strips and in their regularization. This operation encompasses the exclusion of the outliers in the data points, the interpolation of missing points and a final filtering method to properly smooth the profile of the boundaries. The obtained curves are then converted in the original image space and, in the last step, the presence of

reflections and eyelashes that are eventually superimposed to the iris pattern are identified and excluded from the iris segmentation area. In the following sections, each step will be described and detailed.

The proposed method deals with color and grayscale images. In particular, no color-based processing is used since the proposed method exploits only variations in the grayscale image space. Hence, input color images must be converted in the a grayscale image.

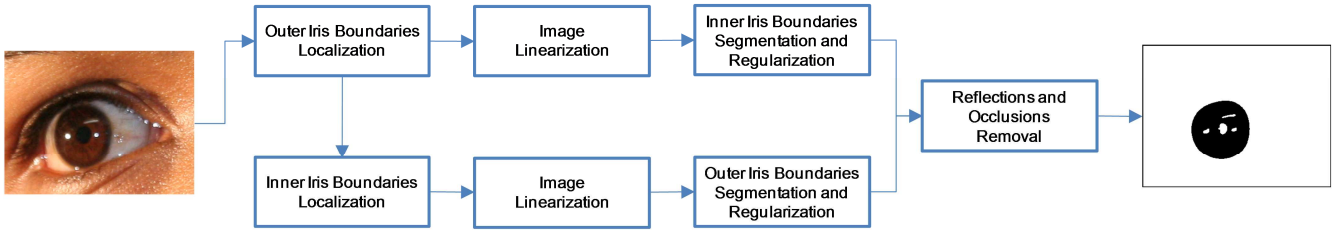

Fig. 2: Structure of the presented method.

2.1 Processing the centers and radii of the inner and outer boundaries of the iris

As a first step, the centers of the inner and outer iris boundary are identified by using a classical method based on a intro-differential technique [4]. The two tasks are processed subsequently: the proposed method provides the localization of the center of the outer iris boundary (the iris-sclera transition), then it estimates the position of the center of the inner iris boundary (the iris-pupil transition) searching in a small region of interest. This image portion has an area of 11×11 pixel and it is located in the estimated center of the outer boundary (Fig. 2). In the literature, other different methods for the location of the iris and the measure of its radius are available, for example the ones proposed in [5-9]. The integro-differental approach aims to find the coordinates of the maximum quantity J obtained by a circular integral centered on the point (x_0, y_0) with radius r of the radial derivate $\partial/\partial r$ of the original image $I(x,y)$, blurred with a gaussian kernel G_σ with spread σ, where

$$J(r, x_0, y_0) = G_\sigma(r) * (d/dr) \oint_{r,x0,y0} (I(x,y)/2\pi r)\, ds\,, \tag{1}$$

$$G_\sigma(r) = \left(1/(\sigma\sqrt{2\pi})\right) \exp(-r^2/2\sigma^2)\ . \tag{2}$$

The search for the maximum of the quantity J is processed in a parameter space bounded by the following limits: $X_{min} \le x_0 \le X_{max}$, $Y_{min} \le y_0 \le Y_{max}$, $R_{min} \le r \le R_{max}$. The bounds X_{min} and X_{max} , Y_{min} and Y_{max} can be associated to the width and the height expressed in pixels of the input image $I(x,y)$, respectively, $R_{min} = 0$ and $R_{max} = \sqrt{{X_{max}}^2 + {Y_{max}}^2}$.

The values of the parameters R_{min} and R_{max} are different in the case of the outer and inner iris boundary segmentation. In the case of the outer iris boundary segmentation for the NICE.I database, R_{min} was empirically set to 50 pixel and R_{max} to 150 pixel (the half of the height of the NICE.I images). In the case of the segmentation of the inner boundary, R_{min} was equal to the 10% of the iris radius, and R_{max} was set equal to the 80% of the iris radius. These percentages was set according to [4].

The σ parameter can be fixed by using a fraction of the image width, or considering a fraction of the maximum allowed radius R_{max}. The choice of σ parameter can be done also by processing a reduced set of images, searching for the best $\bar{\sigma}$ which maximize the quantity J for all r, x_0 and y_0 in Eq. (1). Errors in the estimation of σ values with respect to the optimal value $\bar{\sigma}$

are not particular critical, but, notably, experiments showed that the algorithm has a more robust behavior with σ larger than the optimal setting $\bar{\sigma}$, than vice versa.

The two candidate points related to the inner iris boundary $\{r_p, x_p, y_p\}$ and the outer iris boundary $\{r_i, x_i, y_i\}$ can be obtained by selecting the two highest values of J with a sufficient radius difference ($R_{max}/5$ for the NICE.I database) and taking into account that the pupil data can be easily identified by selecting the minor radius between the two candidates.

In classical applications of iris recognition, the parameter space of the maximization can be efficiently reduced by introducing a priori hypothesis on the input image, typically, it can be done by limiting the range of the possible radii and assuming that the pupil center is close to the image's center in a specific region of interest. These assumptions can be correct in controlled biometric setups, but, differently, in a dataset with noisy images there is typically no a priori knowledge concerning the position of the iris in the image and the diameter of the iris boundaries. As a consequence, a larger parameters space have to be explored. This step of the proposed method is very critical since it is the most computational intensive, and, as further discussed in section 3, failures on the detection of the correct centers can jeopardize all subsequent stages, producing a wrong final segmentation of the iris.

2.2 Iris linearization

This stage of the presented method aims to extract from the input image $I(x, y)$ two image strips containing the boundary of the inner and outer edge of the iris pattern (the S_1 and S_2 strips in Fig. 3). After a linearization operation, these strips will be used to achieve a fine localization of the pixels that lie on the iris boundaries. Fig. 4 shows the main steps of this stage of the proposed method. Each strip is extracted by the radial gradient image $R(x,y)$ processed around the candidate centers previously obtained, in particular the inner strip S_1 will be processed around the candidate point $\{x_p, y_p\}$, and the outer strip S_2 around the candidate point $\{x_i, y_i\}$.

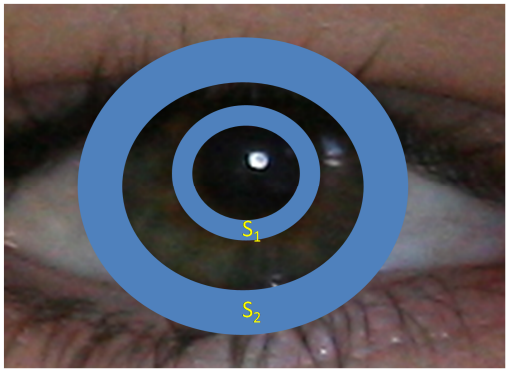

Fig. 3: Extraction of the two strips containing the internal (S1) and external (S2) boundary of the iris

The radial gradient image $R(x,y)$ around a candidate point $\{x_0, y_0\}$ of the input image $I(x,y)$ is processed as follows. The input image $I(x,y)$ is convolved with a classical 3x3 Sobel kernel along the x and y axes, obtaining the x and y components of the gradient image

$$G_x(x,y) = \begin{bmatrix} +1 & 0 & -1 \\ +2 & 0 & -2 \\ +1 & 0 & -1 \end{bmatrix} * I(x,y), \qquad G_y(x,y) = \begin{bmatrix} +1 & +2 & +1 \\ 0 & 0 & 0 \\ -1 & -2 & -1 \end{bmatrix} * I(x,y). \tag{3}$$

The magnitude $G(x,y)$ and phase $\theta(x,y)$ images are then processed as follows

$$G(x,y) = \sqrt{G_x(x,y)^2 + G_y(x,y)^2}\ ,\ \theta(x,y) = \tan^{-1}\big(G_x(x,y)/G_y(x,y)\big)\ . \tag{4}$$

The angle image Ω is created by processing the angle of the straight line passing through the candidate point $\{x_0, y_0\}$ for each pixel $\{x, y\}$ as follows

$$\Omega(x,y,x_0,y_0) = \tan^{-1}[(y-y_0)/(x-x_0)]\ . \tag{5}$$

The final gradient image $R(x,y)$ is obtained by the product of the gradient magnitude image $G(x,y)$ and the cosine of the difference between the two angle images, hence

$$R(x,y)|_{x_0,y_0} = G(x,y)\ \cos(\theta(x,y) - \Omega(x,y,x_0,y_0)). \tag{6}$$

As shown in Fig. 4, the gradient image obtained in Eq. (6) is then cropped separately for the inner and outer image strips. In particular, concerning the pupil, the radial image $R_p(x,y)$ is obtained by centering the derivative operator in $\{x_p, y_p\}$ and forcing to zero the pixels that are outside a distance range $\big[r_p(1-\alpha)\ , r_p(1+\alpha)\big]$ from the center $\{x_p, y_p\}$ as follows

$$\mathrm{R_p(x,y)} = \begin{cases} R(x,y)|_{x_p,y_p} & \text{if}\quad r_p(1-\alpha) \le \sqrt{(x-x_p)^2 + (y-y_p)^2} \le\ r_p(1+\alpha) \\ 0 & \text{otherwise} \end{cases}. \tag{7}$$

Similarly, the same operation is applied to the iris center, obtaining

$$\mathrm{R_i(x,y)} = \begin{cases} R(x,y)|_{x_i,y_i} & \text{if}\quad r_i(1-\alpha) \le \sqrt{(x-x_i)^2 + (y-y_i)^2} \le r_i(1+\alpha) \\ 0 & \text{otherwise} \end{cases}. \tag{8}$$

In Eq. (7) and in Eq. (8), the α parameter was empirically adjusted to 0.3 for the NICE.I dataset.

As a last step of this stage, the obtained images $R_p(x,y)$ and $R_i(x,y)$ are linearized around their center points by using a classical method of linear interpolation achieved by converting the two images from the Cartesian coordinates to the Polar coordinate images $R_p(\rho,\theta)$ and $R_i(\rho,\theta)$ [10]. An example of the two image strips $R_p(\rho,\theta)$ and $R_i(\rho,\theta)$ can be seen in Fig. 4 in output of the *Strip Linearization* module for the corresponding input image.

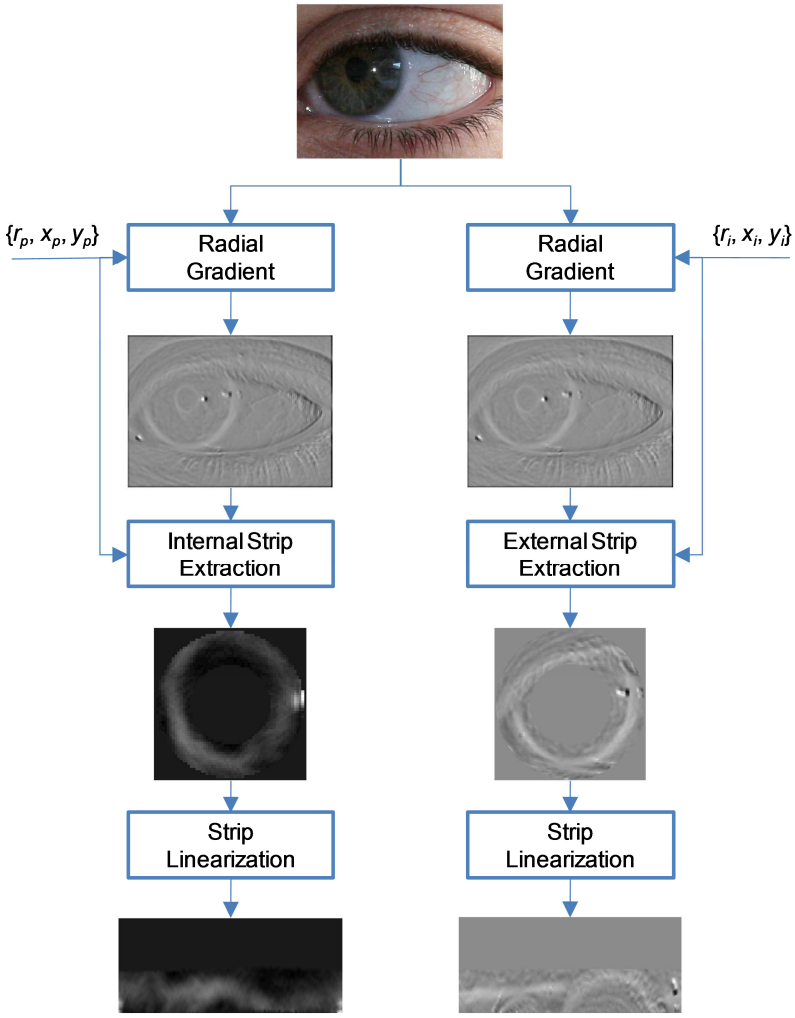

Fig.4: Extraction and linearization of the inner and outer edges of the iris.

2.3 Iris boundaries extraction and regularization

This step of the method aims to identify in each extracted strip $R_p(\rho,\theta)$ and $R_i(\rho,\theta)$ the associated position of the inner and the outer iris boundary, $b_p(\theta)$ and $b_i(\theta)$ respectively. The presence of an iris boundary is related to local maxima along the columns in the strip (the ρ axis) since the radial gradient tends to have high values due to the strong radial transitions in the grey levels images. As a first approximation, the iris boundaries $b_p(\theta)$ and $b_i(\theta)$ are hence extracted by selecting the position of the maximum in each column in the corresponding extracted strip $R_p(\rho,\theta)$ and $R_i(\rho,\theta)$, hence

$$b_p(\theta) = \max_{r_p(1-\alpha)\leq\rho\leq r_p(1+\alpha)} R_p(\rho,\theta)\,, \tag{9}$$

$$b_i(\theta) = \max_{r_i(1-\alpha)\leq\rho\leq r_i(1+\alpha)} R_i(\rho,\theta)\,. \tag{10}$$

The presence of occlusions can strongly impact on the behavior of the maxima extraction method, since the typical radial derivate pattern of the iris is superimposed or substituted with different patterns coming from the reflections and the eyelashes. This presence of occlusions often adds abrupt variations in the iris boundaries, and the resulting reconstructions of $b_p(\theta)$ and

$b_i(\theta)$ can be inaccurate for a large range of θs. Fig. 5 plots an example of the two extracted strips and the corresponding maxima positions in the case of presence of boundaries discontinuities caused by occlusions and reflections.

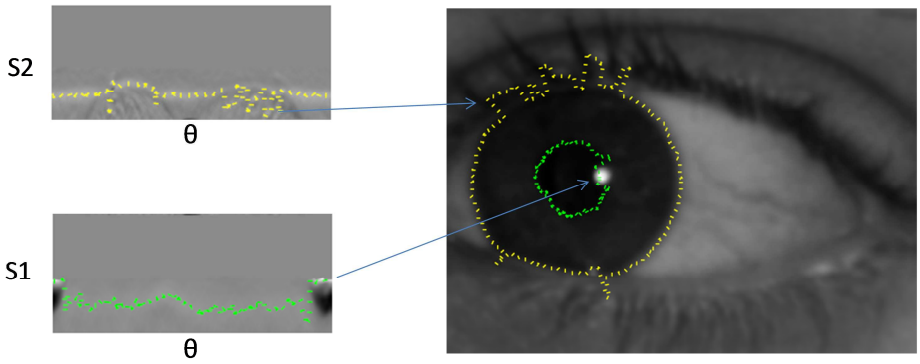

Fig. 5. Wrong identification of the iris boundaries $b_p(\theta)$ and $b_i(\theta)$ using the maxima extraction method. Reflections and occlusions reduce the continuity of the iris boundaries by adding abrupt variations in the radius.

The assumption that occlusions can produce strong discontinuities in the iris boundaries by using the maxima extraction method can be exploited to design a subsequent boundary regularization. Without loss of generality, let us now describe the regularization method for the iris boundary $b_i(\theta)$, similarly the same method can be applied to the pupil boundary $b_p(\theta)$. The method we propose achieves the selection of continuous intervals of the boundary by using a double hysteresis thresholding analysis. Let us assume that are available N values of $b_i(\theta)$ for the corresponding θ values $\{\theta_1, \theta_1, \dots \theta_N\}$, where the parameter N sets the angular resolution of the analysis which is equal to 360/N degrees. The method can be described with the following steps:

1. *Identification of continuous segments* - starting from an angle θ_i, let us consider the following values of $b_i(\theta_j)$ until it holds the following inequality $|b_i(\theta_i) - b_i(\theta_j)| < t_1$, with $i < j$;
2. *Polar continuity control* - if the first point of the first segment and the last point of the last segment satisfy the conditions in Step (1), the vectors are merged;
3. *Length evaluation and storage* - if $j - i > t_2$, the segment is classified as "continuous" and the values $\{b_i(\theta_i), b_i(\theta_{i+1}), \dots b_i(\theta_j)\}$ are added to a vector B, otherwise the segment is classified as "discontinuous" and $j - i$ zeros are added to the vector B;
4. *Loop Termination* - until all available values have been processed, the analysis starts again (Step 1), otherwise the method ends.

The second step of the algorithm is required since the points $\theta_1$and θ_N in the polar representation are not contiguous, but, on the contrary, they are contiguous -by definition- in the Cartesian representation. Hence, it is necessary to verify the continuity condition of the segment obtained by merging the first and the last segments during the process. After the last step, a new iris boundary is available in the vector $B(\theta)$. It contains the continuous segments which have been identified, and -probably- some zero-radius segments where the iris border has been classified as discontinuous.

The last stage of the iris regularization method consists of a low-pass filtering of the obtained boundary vector $B(\theta)$ aiming to smooth the rapid transitions and to guarantee that the final boundary is a close path. In the literature, similar approaches

based on active contours have been studied [11, 12]. The method we propose in this work is based on the analysis of Fourier coefficients [13]: the basic idea is to truncate the Fourier expansion of the boundary $B(\theta)$ in order to achieve the low-pass operation. It is important to note that the Fourier approach can be used since the boundary $B(\theta)$, expressed in polar coordinates, can be considered as a periodic discrete signal (with period N) as a direct effect of its circularity and of the constant angular resolution used for its sampling. In this framework, the signal $B(\theta)$ can be expressed by the Fourier series and the relative set of coefficients

$$C_k = \sum_{\theta=0}^{N-1} B(\theta)\exp\left(-j(2\pi/N)k\theta\right). \tag{11}$$

In order to obtain the desired filtering effect, the regularization boundary can be build by using only the first M Fourier coefficients as follows

$$\tilde{b}(\theta) = (1/N)\sum_{i=0}^{M-1} C_k \exp(-j(2\pi/N)k\theta), \tag{12}$$

where $M<N$. The choice of the number of coefficients M controls the smoothness of the regularized boundary and, hence, the overall behavior of the segmentation algorithm. Similarly, the same method can be applied to the regularization of the inner boundary of the iris $b_p(\theta)$. In Fig. 6 it is plotted the effect of the application of Eq. (12) by using 5 coefficients for the inner and outer boundary of the iris in Polar (Fig. 6a) and Cartesian coordinates (Fig. 6b).

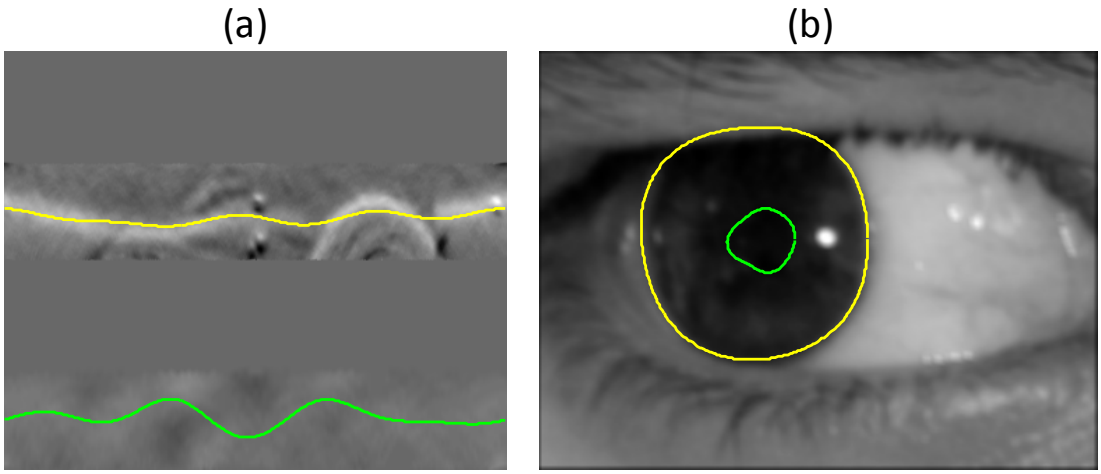

Fig.6: Regularization of the iris boundaries by using low pass filtering.

2.4 Removal of eyelashes/reflections and image reconstruction

In order to complete the segmentation process, the outer and inner boundary of the iris have to be converted again into the Cartesian space, and the remaining occlusions must be removed from the iris pattern. As a first step, the method estimates the presence of eyelashes, then it identifies the presence of the reflections. Finally, the estimated occlusions are then marked and removed from the final segmentation area of the iris.

The localization of the eyelashes can be more accurate by using different models according with the peculiar characteristics of the eyelashes [14, 15]. Typically, the eyelashes can be mainly distinguished in two kinds (Fig. 7): separable eyelashes (each element is distinguishable and separated from the others), and not-separable eyelashes (the image of the eyelashes is confused or blurred and it is not possible to detect the boundaries of each element).

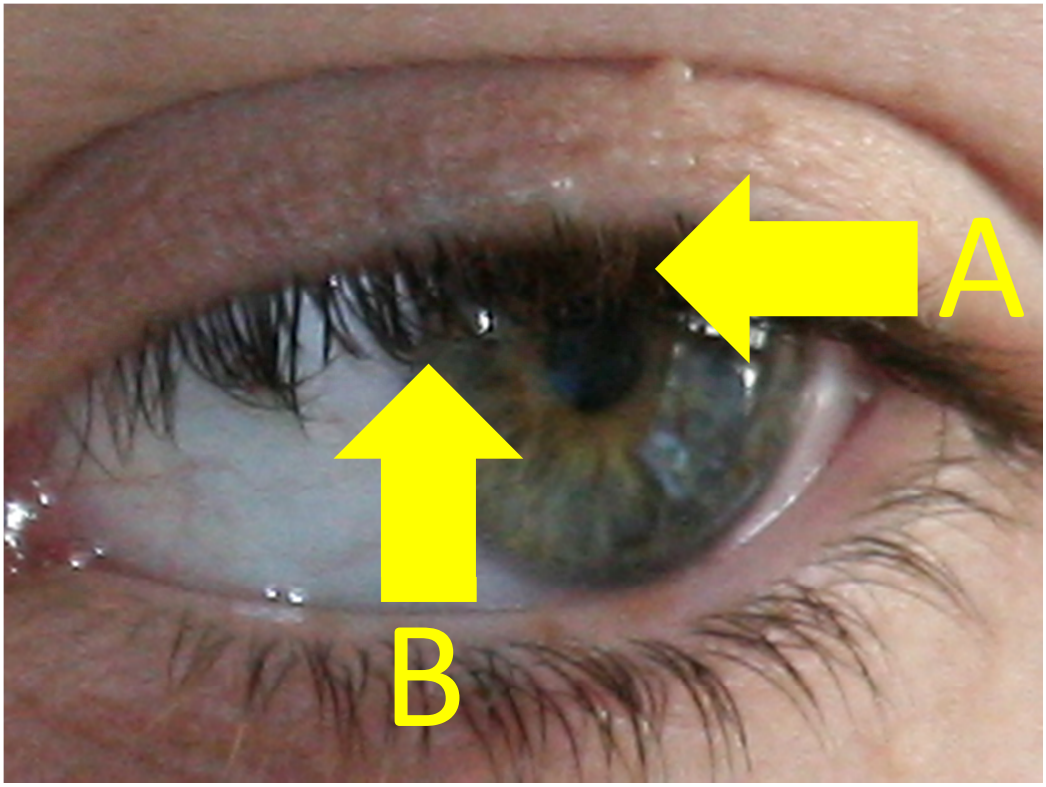

Fig. 7: Eye brushes can be better modeled by considering their differences. In region (A) the image of the eyelashes is fuzzy and they are not separable, in (B) eyelashes elements can be better individuated.

The detection of the separable eyelashes (the region (A) in Fig. 7) has been achieved by using an approach based on Gabor filtering followed by a tresholding method, and a final morphological operation on the resulting image. The Gabor filter operates an enhancement of the regions of the image that have specific angular and frequency characteristics, therefore it is possible to exploit the knowledge of the eyelashes patterns to achieve an effective identification and removal. In particular, it is possible to tune the parameters of the Gabor filter to enhance the patterns associated to thin and long objects that are disposed along the vertical direction (see for example the eyelashes on the top eyelid in Fig. 7). The general expression of the Gabor filter can be expressed as follows

$$g(x,y) = K \exp\big(-\pi(a^2(x-x_0)^2 + b^2(y-y_0)^2)\big) \exp\big(j(2\pi F_0 (x\cos\omega_0 + y \sin\omega_0) + P)\big), \quad (13)$$

where K is the scale of the magnitude the Gaussian envelope, a and b are the scales of the two axes of the Gaussian envelope, x_0 and y_0 are the coordinates of the Gaussian peak, F_0 is the spatial frequency of the sinusoid carrier, ω_0 its orientation, and P its phase shift. The tuning of the filter parameters can not be completely done by using a priory information, and a *trial and*

error approach can be considered in order to optimize the filter behavior on a specific image dataset. In particular, for the NICE.I dataset we used the following values K =1, $a = 0.6$, $b = 0.6$, $x_0 = 0$, $y_0 = 0$, $\omega_0 = 0$, $P = 0$, and $F_0 = 0$.

The real part of the convolution between the input image and the Gabor kernel is an image where the eyelashes tend to assume high intensity values, hence a thresholding method can be used to locate the candidate pixels which belong to the eyelashes. In our approach, the processed image is obtained as follow

$$L_1(x,y) = \begin{cases} 1 & \text{if } \left|I(x,y) * \mathcal{R}e\big(g(x,y)\big)\right| > t_3 \\ 0 & \text{else} \end{cases} \qquad (14)$$
$$t_3 = k \max(|I_r(x,y) * g(x,y)|)$$

where, the threshold t_3 is equal to a fraction of the maximum value of the output of the filter on a reference image $I_r(x,y)$. If one takes the same input image $I(x,y)$ as reference image $I_r(x,y)$, the operation implicitly assumes that at least some portion of eyelashes is present in the image. This working hypothesis is quite reasonable and it is verified in the large majority of the eye images.

In Fig. 8, for an input image (a), the application of the Gabor filter is plotted showing the convolution $I(x,y) * g(x,y)$ (b), and the location of the pixels with intensity values greater than the fixed threshold t_3 (c). The portion of the pixels identified as eyelashes by Eq. (14) is typically over-segmented since many isolated pixels that are not belonging to the eyelashes can marked as eyelashes by the method. In this case, it can be very effective to process a morphological operation on $L_1(x,y)$ in order to remove the isolated pixels that are not connected to larger objects [16, 17].

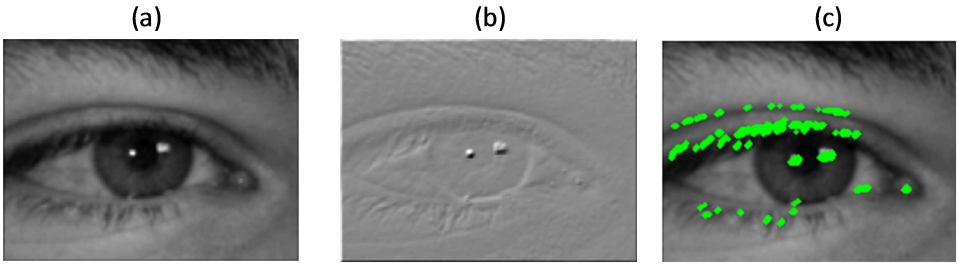

Fig. 8: Application of the Gabor filter for the detection of the separable eyelashes: (a) the input image; (b) the output of the Gabor filter; (c) the segmented image by closing and tresholding.

The localization of not separable eyelashes (the region (B) in Fig. 7) can be achieved by considering a different model. In this case, the eyelashes tend to be grouped in a fuzzy set of lines and it is not possible to adopt a specific approach as in the previous case. In the literature, statistical approaches have found to be more effective and, in addition, they can be exploited also for the detection of external reflections [16]. This approach is based on the fact that high values of the local variance of the images are associated to the presence of eyelashes and reflections in the input image. As a consequence, the identification can be achieved by a thresholding method as follows,

$$L_2(x,y) = \begin{cases} 1 & \text{if } \operatorname{var}\big(I(x,y)\big) > t_4 \\ 0 & \text{else} \end{cases}, \qquad (15)$$

where the local variance is processed in a 3×3 matrix centered on the current pixel (x,y) and it is compared to a fixed threshold t_4. The threshold t_4 can be tuned according the current dataset as a fraction of the maximum variance present in the images. This operation tends to produce a large amount of isolated pixels that are not associated to reflections or eyelashes (false positive cases). This drawback can be effectively reduced by adopting a morphological erosion operation as follows

$$L_3\,(x,y) = \mathrm{erode}(L_2(x,y), S\,), \tag{16}$$

where S is the erosion structuring element [18] which has to be tuned according to the dataset. Working with the NICE.I dataset, we found that a structuring element of 2×2 pixels offers a proper tradeoff between the number of false positive and false negative in the identification of the occlusions in the iris region.

Strong and large reflections cannot be correctly detected with the previous method since the local variance is very low. This kind of reflections tends to occur close to the center of the iris pattern and it is very bright in intensity. Based on this observation, it is possible to create a new segmentation mask for strong reflections by exploiting a direct thresholding method on the gray level of the input image as follows

$$L_4\,(x,y) = \begin{cases} 1 & \text{if } I(x,y) > t_5 \\ 0 & \text{else} \end{cases}, \tag{17}$$

where the threshold t_5 can be fixed as a fraction close to the maximum value of intensity present in the image (the saturation value for the NICE.I dataset).

In order to correctly fuse the data present in each segmentation mask (L_1: separable eyelashes, L_3: non separable eyelashes and weak reflections, L_4: strong reflections) we propose the following approach. Starting from an initial set of points $L_5 = L_3$ OR L_4 we apply an iterative region growing technique based on the following condition

$$\mu + \beta\sigma < I(x,y), \tag{18}$$

where μ and σ are the local mean and standard deviation of $I(x,y)$ processed in a 3×3 matrix centered in the point (x,y). The β parameter is a weight factor that must be tuned with respect to the current image dataset (in the case of NICE.I dataset we set $\beta = 2$). The condition in Eq. (18) is tested for each pixel belonging to the connected elements present in L_5 until no more boundaries pixels satisfy the condition. All pixels satisfying the condition in Eq. (18) during the iterations are marked in a final mask L_6 representing the complete occlusions map. Fig. 9 plots two examples of the application of the proposed method: it can be seen that the proposed method correctly segments the eyelashes and reflections, but it produces a large number of false positive pixels outside the iris pattern. This behavior does not represent a problem since the iris boundaries were already detected using the method in Eq. (12), and, hence, all the points identified as eyelashes and reflections outside the iris pattern will be discarded. With specific reference to the detection and removal of the iris reflections, different methods can be also found in [19,20].

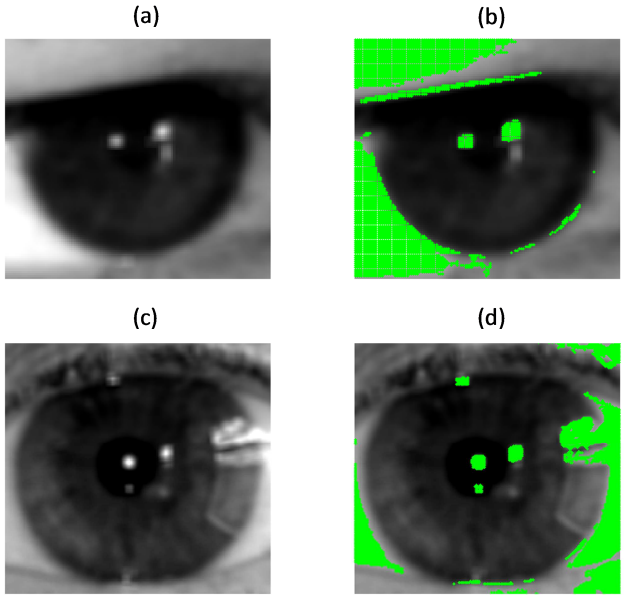

Fig. 9: Detection of non separable eyelashes and reflections by a statistical approach: the local variance of the input images is adaptively thresholded and eroded in order to identify the occlusions and reflections in the iris pattern. Subplots (a) and (c) show the central portion of two starting images. Subplots (b) and (d) show the output of the algorithm in the case of non-separable eyelashes and large reflections, respectively.

3 EXPERIMENTAL RESULTS

The presented approach was tested on the NICE.I and CASIA-IrisV3-Interval datasets [21]. The NICE.I dataset is composed by 488 color images taken at visible wavelength with the image size of 400×300 pixel. Associated to each image, the dataset provides the binary map of the correct iris segmentation. The CASIA-IrisV3-Interval dataset is composed by 2655 images acquired at infrared wavelength with the image size of 320×280 pixel. All presented algorithms have been written in Matlab language (Version 7.6) exploiting the available toolboxes [22].

On a Intel Core Duo 2.4GHz working with Windows XP, the overall processing time for 1 image is about 3 minutes. The profiling analysis showed that 98% of the computational time is required to process the identification of the initial points using Eq. (1). An optimization of the method described in Eq. (1) could hence provide strong improvements in the overall computational time.

The accuracy of the segmentation method can be evaluated with different figures of merit. The most complete measure is the *total classification error* that is the amount of pixels in the dataset misclassified by the proposed method. In addition, the mean value of the *pixel error* estimates very well the probability of classification error of the method in this specific applicative context. The proposed method has been independently tested by the NICE.I organizes on a "fresh" dataset (never used to tune system's parameters) achieving a classification error equal to 3.01% (False Positive ratio = 1.9%, False Negative ratio =21.3%). This independent procedure of evaluation offers a fair estimation of the real generalization capability of the method.

The behavior of the proposed method can also be qualitatively studied by analyzing the distribution of the classification errors directly in a subset of images. Fig. 10 plots the 19 images with the highest classification error per image, where the black areas in the iris are related to correct classification, pale green areas are related to false positive errors, and dark red areas represent false negative detections. The analysis of the error regions in the images enlightens the dependence of the segmentation error on two main factors. The first is the dependency of the errors with respect to the radius of the iris. In particular, the behavior of the method worsens for large irises (close up images). The second factor is related to the presence of glasses (the last two columns). In this case, the method tends to produce wrong estimations of the initial center points of the iris and the pupils, and hence it produces segmentation outputs which are completely failed. In both cases, the errors are related to a poor initial estimation of the centers/radii of the iris boundaries. As a consequence, false positive and false negative errors are both present.

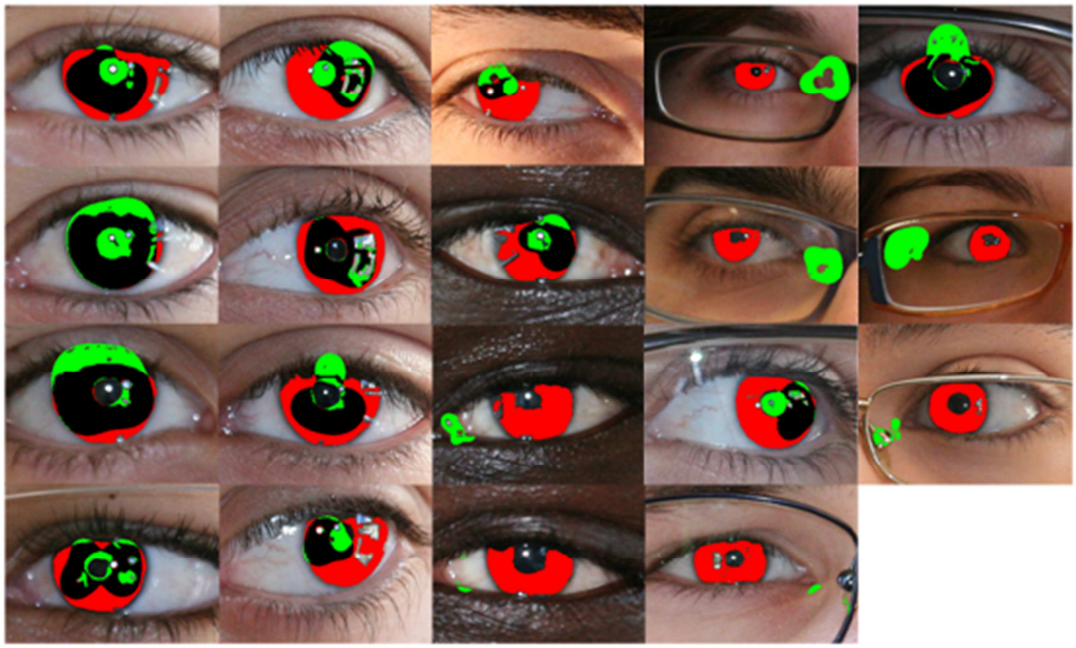

Fig. 10: worst 19 segmentation cases in the NICE.I evaluation.

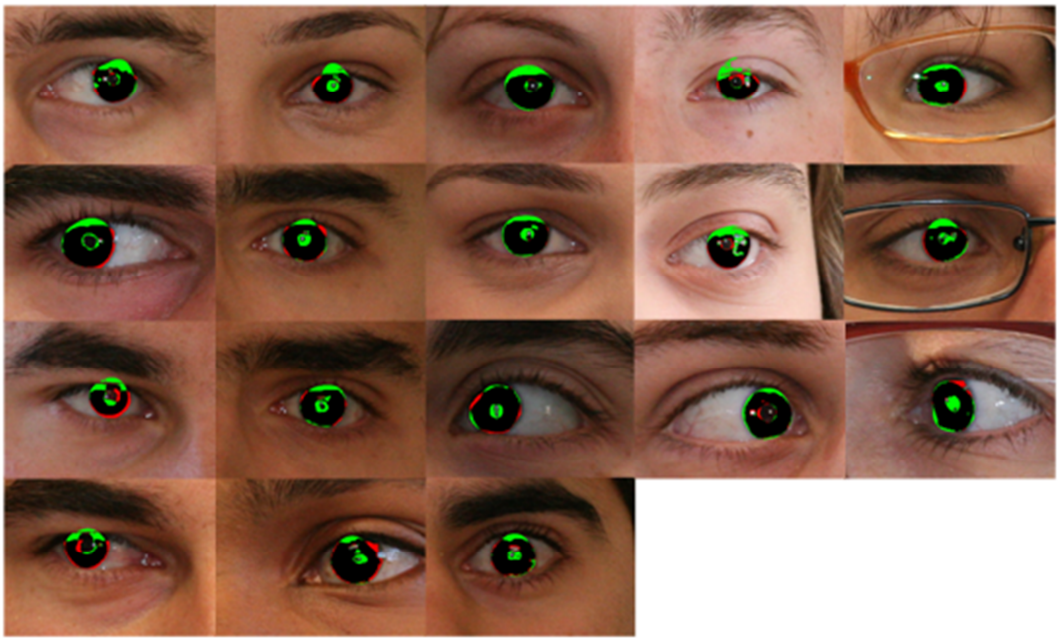

Fig. 11: best 18 segmentation cases in the NICE.I evaluation.

Fig. 11 plots the 18 image of the NICE.I dataset with lower classification errors. It can be noted that the presence of glasses (the three subplots in the last column) does not affect the behavior of the proposed method in this set of images. Moreover, the method has a correct behavior with irises in different positions in the eye, and the distributions of false positive and false negative errors is not equal since the former are much more frequent than the latter. This is related to the fact that the segmentation method tends to overestimate the iris border on the upper side (all subplots in the first two rows present this behavior). Improvements of the eyelashes detection method are hence need, as well as the adoption of a new method to estimate the presence of eyelids.

We tested the proposed method also using the CASIA dataset. This dataset does not provides any supervised information concerning the iris segmentation area of each image, since we used the CASIA dataset only to qualitatively evaluate the iris segmentation capability of the proposed method and its robustness if applied on different image types. Results indicate that the presented method can efficiently work also on different dataset and image types, but a fine tuning of its parameters is strongly needed in order to guarantee a satisfactory behavior. Future works are needed to study more specific adaptive thresholding techniques and then improving the generality of the proposed approach, with particular reference to the initial estimation of the centers of the inner and outer boundaries of the iris.

4 CONCLUSIONS

The paper presented an innovative composition of algorithms for the segmentation of iris images captured in noisy environments. In particular, the proposed method can deal with different images sizes, colors and tones of the skin, positions of the iris in the eye, different illumination systems, and occlusions such as eyeglasses, eyelashes, eyelids. The segmentation

output is refined exploiting a regularization method for the internal and external boundaries of the iris and removing the occlusions such as eyelashes and reflections that are eventually superimposed to the iris pattern.

Results indicate that the proposed approach is effective and it is suitable to deal with the iris acquisition in noisy environments. In particular, the parameters of the algorithm have been optimized for the NICE.I dataset, but the presented approach is general and can be applied to a great variety of iris images. The method described in this paper ranked seventh in the international Noisy Iris Challenge Evaluation (NICE.I) with 97 registered participants among universities and companies of more than 30 countries achieving an overall segmentation error of 3.01%.

Experiments enlightened that the performance of the method is mainly related to the correctness of the initial estimation of the centers of the inner and outer boundary of the iris. Notably, the most important segmentation error factors are related to the failures on this stage. Almost certainly the performance of the presented method can be further improved by applying more robust algorithms to find a correct approximation of the starting points.

REFERENCES

[1] A. K. Jain, Ruud M. Bolle, Biometrics: Personal Identification in Networked Society, Springer, 2007.

[2] J. Jang, K. Kim, Y. Lee, Efficient Algorithm of Eye Image Check for Robust Iris Recognition System, in: Lecture Notes in Computer Science v2756, Springer Berlin Heidelberg, 2003, pp. 301-308.

[3] Hugo Proença, Luís A. Alexandre; The NICE.I: Noisy Iris Challenge Evaluation - Part I, in Proceedings of the IEEE First International Conference on Biometrics: Theory, Applications and Systems - BTAS 2007, Washington DC, U.S.A., September 27-29, 2007, ISBN: 978-1-4244-1597-7.

[4] John Daugman: How iris recognition works. IEEE Trans. Circuits Syst. Video Techn. 14(1): 21-30 (2004)

[5] X. He, P. Shi, A new segmentation approach for iris recognition based on hand-held capture device, Pattern Recognition 40 (2007) 1326-1333.

[6] R.M. Gaunt, D.M. Etter R.W. Ives, L.R. Kennell, IEE Conference Record of the Thirty-Ninth Asilomar Conference on Signal, Systems and Computers (2005) 859- 863.

[7] R. P. Wildes, Iris recognition: an emerging biometric technology, Proceedings of the IEEE 85 (1997) 1348-1363.

[8] L. Masek, Recognition of human iris patterns for biometric identification, University of Western Australia, 2003.

[9] W. W. Boles and B. Boashash. A human identification technique using images of the iris and wavelet transform. IEEE Transactions on Signal Processing 46 (1998) 1185–1188.

[10] Park, W.; Chirikjian, G.S., Interconversion between truncated cartesian and polar expansions of images, IEEE Transactions on Image Processing 16 (2007) 1946 -1955.

[11] A. Ross, S.Shah. Segmenting non-ideal irises using geodesic active contours, IEE Biometric Consortium Conference (2006) 1-6.

[12] D. L. Soldan, R. W. Ives R. P. Broussard, L. R. Kennell. Using artificial neural networks and feature saliency techniques for improved iris segmentation, Proceedings of International Joint Conference on Neural Networks (2007) 1283-1288.

[13] J. Daugman, New methods in iris recognition, IEEE Transactions on Systems, Man and Cybernetics 37 (2007) 1167-1175.

[14] Z. Wei, T. Tan, Z. Sun, J. Cui, Robust and fast assessment of iris image quality, in: : Lecture Notes in Computer Science v3832, Springer Berlin Heidelberg, 2005, pp. 464-471.

[15] W.K. Kong, D. Zhang, Accurate iris segmentation based on novel reflection and eyelash detection model, IEEE Proceedings of 2001 International Symposium on Intelligent Multimedia, Video and Speech Processing (2001) 263-266.

[16] R.C. Gonzales, R.E. Woods, Digital Image Processing, third ed., Prentice Hall, Upper Saddle River, 2007.

[17] J.Z. Huang, Y.H. Wang, J.L. Cui, T.N. Tan, Noise Removal and Impainting Model for Iris Imag, Proceedings of IEEE International Conference on Image Processing (2004) 869-872.

[18] H.J.A.M. Heijmans, Composing Morphological Filters, IEEE Transactions on Image Processing 6 (1997) 713-723**.**

[19] F. Scotti, Computational intelligence techniques for reflections identification in iris biometric images, CIMSA 2007, IEEE International Conference on Computational Intelligence for Measurement Systems and Applications (2007) 84-88.

[20] Z. Zhang e Y. Ma G. Xu. Improving the performance of iris recognition system using eyelids and eyelashes detection and iris image enhancement, ICCI 2006, 5th IEEE International Conference on Cognitive Informatics (2006) 871-876.

[21] P.J. Phillips, K.W. Bowyer, P.J. Flynn, Comments on the CASIA version 1.0 iris data set, IEEE Transactions on Pattern Analysis and Machine Intelligence 29 (2007) 1869-1870.